LANGMUIR Article
Cite This: Langmuir 2018, 34, 8393−8399
pubs.acs.org/Langmuir

Conformations and Dynamic Transitions of a Melittin Derivative That Forms Macromolecule-Sized Pores in Lipid Bilayers

Anna E. Pittman,[†] Brendan P. Marsh,[§,†] and Gavin M. King*[,†,‡]

[†]Department of Physics and Astronomy and [‡]Department of Biochemistry, University of Missouri—Columbia, Columbia, Missouri 65211, United States

Supporting Information

ABSTRACT: Systematically evolved from the primary active component of bee venom, MelP5 is a lipophilic peptide with important physical properties that differ from wild-type melittin, including the ability to create large equilibrium pores in lipid bilayers at low peptide to lipid ratios. Self-assembly into stable membrane spanning pores makes MelP5 a promising candidate for future applications in the pharmaceutical arena. Despite significant interest, little is known about the mechanism by which MelP5 remodels the lipid bilayer upon binding. We demonstrate by direct atomic force microscope imaging of supported lipid bilayers in solution that MelP5 remodels 1-palmitoyl-2-oleoyl-*sn*-glycero-3-phosphocholine (POPC) in one of two ways. It creates either highly localized voids in the bilayer or diffuse nonlocalized thinning. Thinning of the bilayer was measured to be 3.0 ± 1.4 Å (mean ± standard deviation) below the surface of the upper leaflet of the bilayer. Pores, defined as highly localized voids in the bilayer, exhibited several sizes. Approximately 20% of pores exhibited large footprint areas (47 ± 20 nm^2) which appear capable of passing bulky macromolecules. The peptide-effected bilayer was observed to reversibly exchange between membrane-thinned and pore states in an apparent dynamic equilibrium. Analysis of time-lapsed images suggested upper and lower bounds ($0.2 < \tau < 180$ s) on the characteristic time scale of transitions between the membrane-thinned and pore states. Moreover, pores were found to colocalize with membrane-thinned regions, a novel observation that is consistent with the notion of cooperativity among membrane-bound peptides when forming pores.

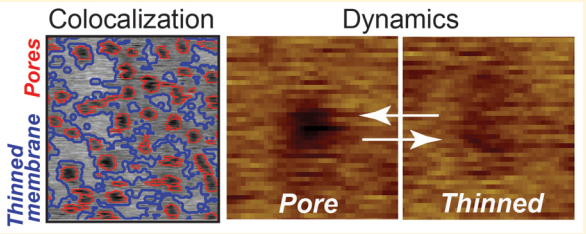

INTRODUCTION

Polypeptide chains that bind to and subsequently form pores in membranes have garnered significant attention in fields ranging from fundamental biophysics to biotechnology.[1] Such pore-forming peptides have significant promise in medicine as direct antimicrobial agents as well as for drug delivery vehicles, including for targeted cancer therapy.[2−4] Notwithstanding their potential, the complex modes of action and dynamic structure of these lipophilic peptides remain poorly understood. To develop more effective therapies and to inform development of novel pore-forming peptides, a more quantitative and mechanistic understanding of peptides interacting with near-native membranes is needed.[5−7]

Pore formation by lipophilic peptides has been investigated by several methods, including circular dichroism, lamellar X-ray diffraction, and surface-induced fluorescence.[8,9] A model system for these studies is the melittin peptide, a chain of 26 amino acids that is the primary toxic component of honey bee venom. Melittin is widely known to affect cell membranes by forming pores, but its effect is short-lived, owing to the inherent instability of the pores.[10−13]

Wild-type melittin is known to have a bimodal interaction with a lipid bilayer; it can exist either in a surface-bound state, with its backbone approximately parallel to the membrane surface, or in an inserted state, forming pores that span the membrane. An amphipathic helix arises when melittin contacts the membrane.[14−16] Furthermore, evidence shows that the percentage of peptides in each state is a function of the peptide-to-lipid ratio.[17] At low peptide concentrations, the majority of peptides associate with their backbones parallel to the membrane; this binding can locally displace lipid head groups, causing a thinning of the membrane (a few angstroms for wild-type melittin).[9] At higher peptide concentrations, the amino acid chains are thought to insert themselves into the membrane and create transmembrane pores.

To improve upon the shortcomings of wild type, a variant of melittin, MelP5, was synthetically evolved to create stable pores with radii large enough to pass macromolecules and to do so at lower peptide concentrations than are required for wild-type melittin.[18] Molecular dynamics simulations of the MelP5 mutant have suggested that this gain of function variant works in a similar fashion to the wild-type peptide.[19] MelP5-induced membrane pores have been studied by electrochemical impedance spectroscopy, macromolecule leakage assays, and single ion channel recording, but the dynamic

Received: March 11, 2018
Revised: May 24, 2018
Published: June 22, 2018

DOI: 10.1021/acs.langmuir.8b00804
Langmuir 2018, 34, 8393−8399

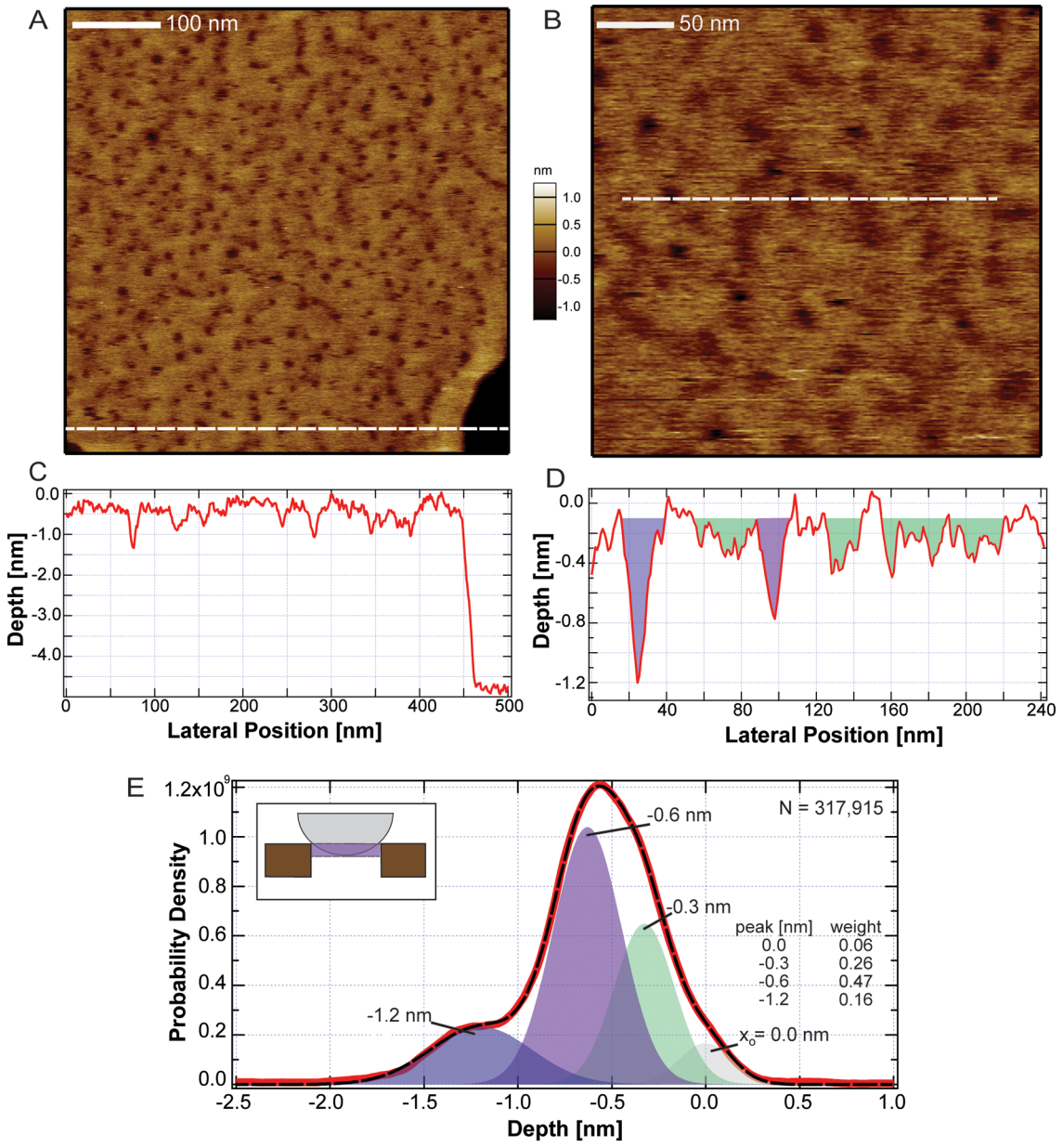

Figure 1. Experimental overview. (A, B) Representative images of the membrane affected by MelP5. (C) Line scan from image in (A), position indicated by dashed line; note the characteristic 4 nm thickness of the bilayer. (D) Line scan taken from image in (B), with certain topographic populations highlighted. (E) Histogram compiled of pixels from representative images taken from three independent experiments. Data are shown in red, and the sum fit is the black dashed line. (E, inset) Cartoon showing an explanation for a shallow reading.

topographic structure of MelP5-induced membrane remodeling remains uncharacterized.[12,18]

Atomic force microscopy (AFM) is a powerful single molecule tool that provides a real-time real-space view of membrane topography with potentially subnm lateral resolution.[20,21] This method allows for direct imaging of peptide-induced remodeling of a fluid lipid bilayer in near-native conditions and has been used to observe defects induced by wild-type melittin.[22] This capability opens the door for studies of nuanced effects, such as the colocalization of the thinning of the bilayer and pores, which can go undetected by other methods.

Here we employed AFM imaging to study the interaction of MelP5 with supported POPC lipid bilayers. MelP5 created stable, highly localized pore-like voids in the membrane with diameters out to around 80 Å. Bilayer remodeling was observed in two distinct modes: shallow nonlocalized thinning or deep highly localized voids. MelP5 exchanged between these two states reversibly in an apparent dynamic equilibrium. Further, the two states were found to be colocalized.

RESULTS AND DISCUSSION

Overview of Atomic Force Microscope Imaging. We studied the topographical consequences of MelP5 binding to lipid bilayers. To this end, we performed tapping mode AFM imaging of supported bilayers made from liposomes which had been incubated with peptides prior to fusion onto mica supporting surfaces.[23] 1-Palmitoyl-2-oleoyl-*sn*-glycero-3-phosphocholine (POPC) was chosen as a model bilayer due to its prevalence in many eukaryotic cellular membranes.[7,24,25]

DOI: 10.1021/acs.langmuir.8b00804
Langmuir 2018, 34, 8393−8399

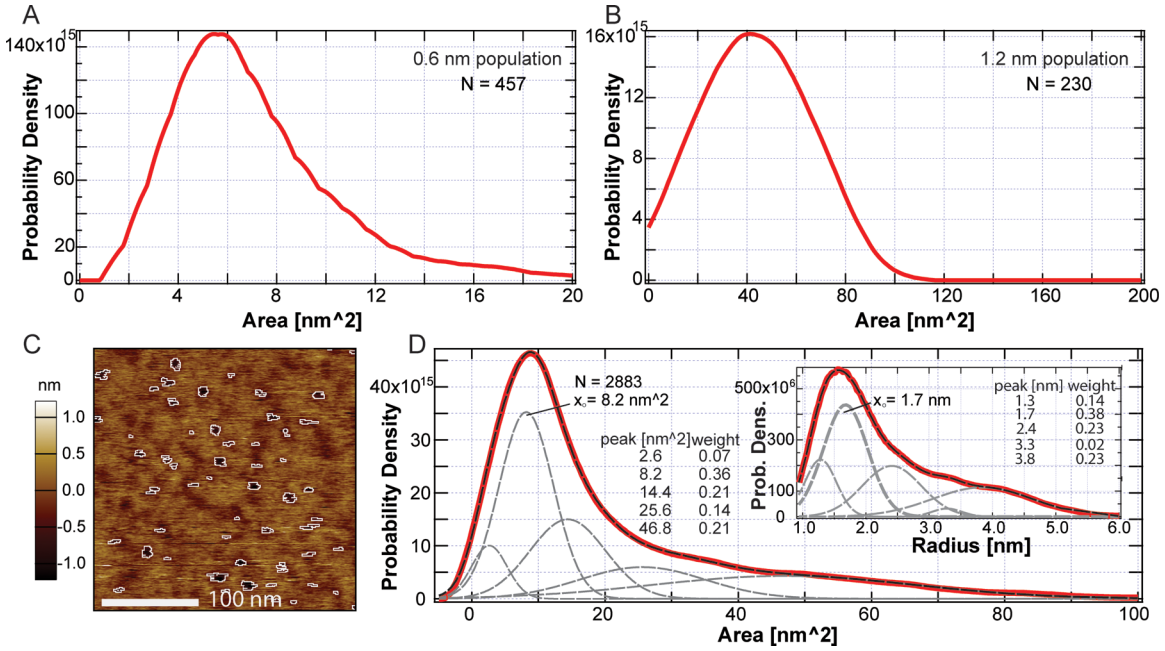

Figure 2. Geometric analysis of pores. Histograms of footprint areas constructed from subpopulations of voids exhibiting depths of (A) -0.6 ± 0.1 nm or (B) -1.2 ± 0.1 nm. In both cases, the distributions are sharply peaked, indicating that these features are highly localized. (C) The program picked out exclusively the pores (white contours) and did not analyze the thinned portions of the membrane. (D) Histogram of footprint areas for all pores. The histogram has a major population at an area of 8.2 nm^2 but has subpopulations that go out as far as 46.8 nm^2. The weight of each peak is listed (gray dashed indicate the Gaussian fits). The data are shown in red, while the dashed black line is the sum fit. Inset: histogram of pore radii.

Previous studies have shown that MelP5 affects lipid bilayers at a variety of concentrations, including significantly lower than those required for wild-type.[18] AFM imaging trials were conducted at varying concentrations of MelP5. Conditions were optimized to yield a significant number of topographic features while simultaneously avoiding large-scale destruction of the membrane. Experiments at high peptide-to-lipid ratios (P:L = 1:250 or 1:120) led to widespread membrane distortion (Supporting Information Figure S1), whereas trials at lower concentrations led to too few features for statistical analysis. It was found that P:L = 1:1200 was optimal for our study, which focused on characterizing the topography and dynamics of MelP5-induced membrane remodeling. We note that trials with wild-type melittin were also carried out, but none of them resulted in the formation of stable porelike features (Figure S2).

Figure 1A shows a representative image of the effects of MelP5 on POPC (500 × 500 nm^2, P:L = 1:1200). Numerous punctate depressions in the membrane surface are visible. A line scan through the image (Figure 1C, white dashed in Figure 1A) reveals the depth of several depressions and verifies the presence of the lipid bilayer via its characteristic 40 Å thickness.[26] As a control, membrane samples prepared in an identical manner, but without MelP5, were shown to be essentially featureless (Figure S3). Figure 1B is an image of MelP5-treated membrane at increased magnification (290 × 290 nm^2). The associated line scan (Figure 1D) highlights two localized pore-like features (purple shades) as well as a diffuse region of thinned membrane (green). Note that the vertical scale in the images (Figure 1A,B) is distinct from the line scans (Figure 1C,D); zero depth in the line scans delineates the top surface in the images, which we take to be the surface of the unmodified upper leaflet of the bilayer. Clearly, MelP5 has a significant effect on membrane topography.

To quantify the distribution of topographic distortions further, a histogram from data acquired in the membrane region of the image (excluding the underlying mica surface) was compiled. This histogram of pixel weights (Figure 1E) reveals several important topographic populations. There appears to be one prominent state exhibiting a depth of -0.3 ± 0.2 nm (mean $\pm \sigma$) below the top of the bilayer, and two other states with depths of -0.6 ± 0.2 and -1.2 ± 0.3 nm. These populations are robust; the histogram (Figure 1E) was compiled using data from three independent experiments (Figure S4).

In terms of relative weights, the 0.6 nm deep state was the most common topographical distortion observed at this P:L = 1:1200. It occurred with a probability per area approximately 3-fold higher than the deeper 1.2 nm state. The 0.3 nm deep state of the membrane was found with an intermediate probability. To summarize, direct inspection of AFM images coupled with histogram analysis of image pixels identified distinct topographic states of MelP5-induced membrane distortion as well as relative weights.

Characterizing Porelike Voids in the Bilayer. To further elucidate the size and form of the voids, these porelike features were isolated algorithmically. Images were analyzed using custom software that located voids in a given image with depths greater than 0.3 nm, controlled by the blob strength parameter in the Hessian blob algorithm.[27] We explored the relationship between measured void depth and footprint area.

By their nature, pores are highly localized voids within an otherwise planar bilayer surface. Both the shallow (-0.6 ± 0.1 nm) and the deep (-1.2 ± 0.1 nm) subpopulations of voids exhibited sharply peaked footprint area histograms (Figure 2A,B). If these two populations represented a deep mode of nonlocalized membrane thinning, then one would expect no underlying structure and no preferred footprint area. In

DOI: 10.1021/acs.langmuir.8b00804
Langmuir 2018, 34, 8393−8399

contrast, the data indicated that both of these void populations were highly localized and hence porelike. Deeper pores exhibited larger areas. Because of their localized nature, different depths could arise from pores with different diameters. This is because the tip would read a shallower depth for a smaller diameter pore (Figure 1E, inset). Because of sharpness and aspect ratio limitations of the AFM probe (Figure S5), the tip was not able to penetrate deeply into the MelP5 pores. However, the underlying structure of the 0.6 and 1.2 nm deep features revealed by area analysis suggests that these two populations are indeed pores.

Once identified (Figure 2C, white contours), a complete histogram of footprint areas was compiled for all pores (Figure 2D). Assuming a circular geometry, which matched many of these features, a histogram of radii was also created (Figure 2D, inset). As seen in Figure 2D, the two most prominent populations of footprint area for MelP5 pores were 8.2 ± 4.1 and 14.4 ± 5.7 nm^2. These populations give rise to radii of 1.7 ± 0.4 and 2.4 ± 0.5 nm, respectively. This geometry is in overall agreement with previous results, which put the radius of MelP5 pores at ≥2 nm due to its release of 10 kDa dextran.[18] Though these two populations together constituted more than half of all the porelike features observed, a significant population (23% of total) exhibited a larger radius of 3.8 ± 0.8 nm. Given the challenges in measuring pore geometry via AFM,[28] the radii and footprint areas reported here are taken to be an upper limit on the narrowest constriction of the pore. In summary, MelP5 does not create one size of pore but rather has a variability of pore footprint areas. This observation, which is based on direct imaging of bilayer topography, is consistent with recent electrophysiology results,[12] though Fennouri et al. employed bilayers from mixed lipid species and here we used POPC.

Characterizing Thinned Regions of the Bilayer. Spatially inhomogeneous and delocalized thinned regions of the membrane were frequently observed in the AFM images. The thinned areas of the membrane had shallower depths and dynamic, less definite structure as compared to the highly localized pores. Thinned areas of the membrane were selected algorithmically in order to more precisely define their structure. Then, a histogram was compiled using only the affected segments of the membrane. As seen in Figure 3, the most probable depth of the thinned area was −0.30 ± 0.14 nm. This agrees with and refines the −0.3 ± 0.2 nm peak identified in Figure 1. Tip restricted depth readings were less of a concern here, since the thinned portions were not deep and exhibited significantly larger areas as compared to both the pores and the apex area of the AFM tip itself. However, we note that while thinned regions with small areas were rare (see Figure 4), they could not be differentiated from pores, given the limitations imposed by tip geometry.

The thinned features were characterized by their footprint area to ascertain if they were indeed thinned only—exhibiting no underlying structure—or if they were pores—which exhibit a high degree of localization. Analyzing the area histogram of the thinned features revealed a wide variety of possible footprint areas; the histogram for the thinned population has a shoulder much larger than the sharply peaked pore histogram. This difference in underlying structure is seen in Figure 4, where integrals of the two area histograms are plotted. For the pores, the integral reaches unity very quickly—indicating that the vast majority of footprint areas are localized in a distinct peak. However, for the thinned areas, the integral does not saturate nearly as rapidly, owing to a lack of underlying structure.

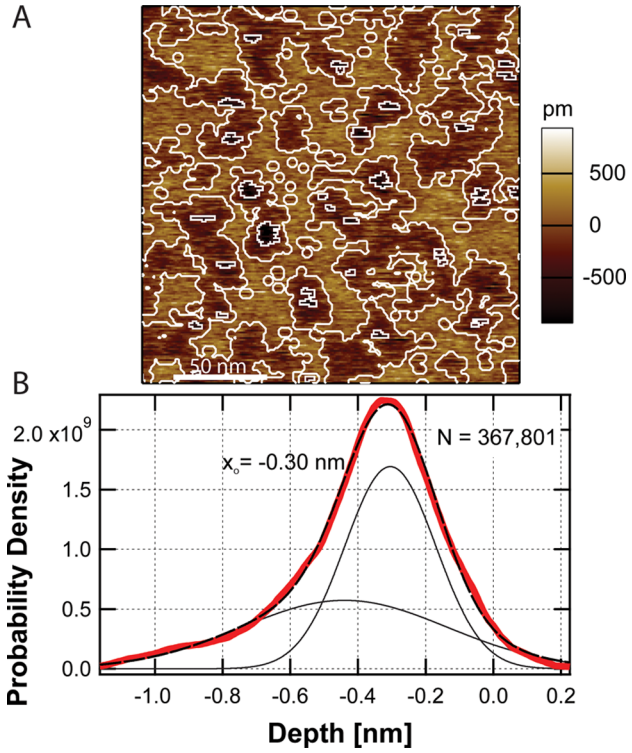

Figure 3. Analysis of thinned regions of membrane. (A) Thinned regions were identified algorithmically and differentiated from taller regions of the bilayer and deeper porelike structures. (B) Histogram of the thinned region exhibiting a peak at −0.30 ± 0.14 nm.

Additionally, for each image there was on average 59 thinned features that accounted for 37% of the total area of the image and 190 pores that accounted for only 3% of the total area of the image (Figure 4B). The membrane-thinned features were therefore much larger in area than the porelike features.

Colocalization of Thinned Membrane Regions and Pores. When analyzing the spatial distribution of the pores and the thinned portions of the membrane, we discovered that pores were always surrounded by or immediately adjacent to thinned areas of the membrane. Figure 5 shows representative images from three separate preparations highlighting this observation. Here the pores are circled in white and the thinned areas in red. In a popular model of pore formation,[17] pores form in regions where enough peptides have already congregated and thinned the membrane; this membrane-bound pool of peptides can then act in a cooperative manner to form a pore. We emphasize that the observation of colocalization between membrane thinned regions and pores requires a single molecule approach. Using the AFM, we were able to directly image the colocalization and thus shed light on the process of cooperativity. Previous studies have shown that wild-type melittin can thin the bilayer,[9] but the lateral distribution and location of the thinning and how it relates to pore location remained unknown. We observed that MelP5 causes laterally disperse and inhomogeneous thinning of the bilayer and that these thinned regions have within or abutting them punctate pores.

Topographical Dynamics: Transitions between Membrane-Thinned States and Pore States. Continuously imaging the same area of the lipid bilayer surface gave us

DOI: 10.1021/acs.langmuir.8b00804
Langmuir 2018, 34, 8393−8399

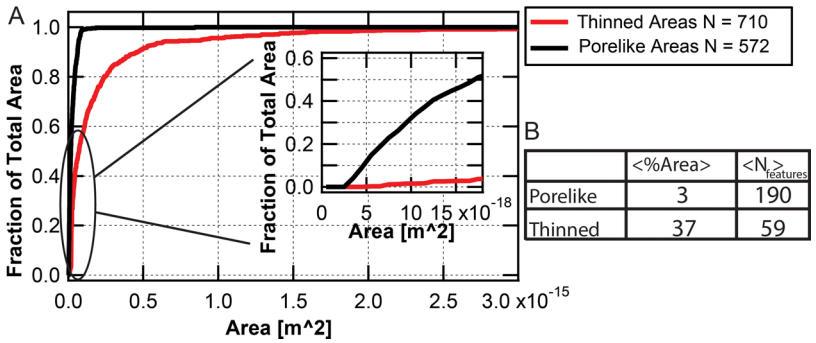

Figure 4. Comparison of areas. (A) Integrated area histograms for both the porelike features (black) and the thinned features (red). Inset: a detailed view highlights the difference between the two populations. (B) Table comparing the pores and thinned features of the membrane. Two quantities are of interest: (i) the average percent area of an image taken up by the pores or the thinned features and (ii) the average total number of each feature type per unit area.

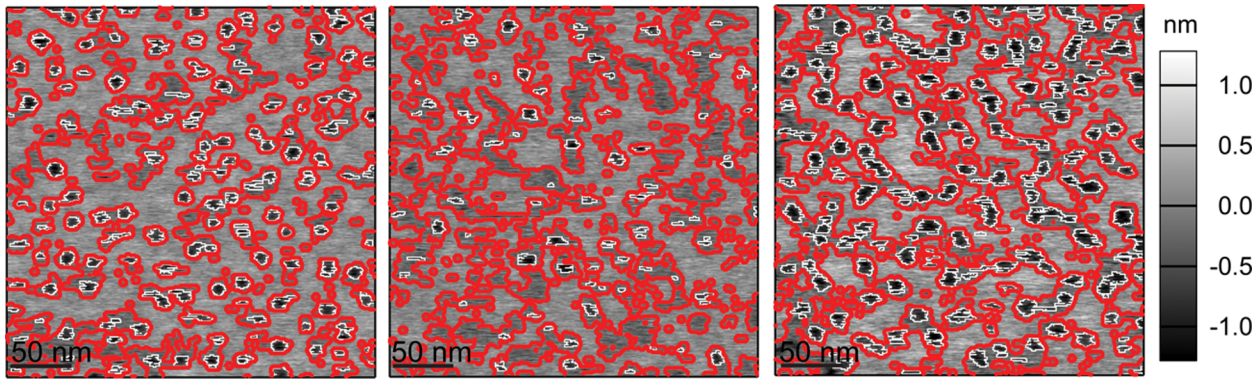

Figure 5. Colocalization of pores and membrane-thinned regions. Images of bilayers with MelP5 show that the pores (circled in white) fall within the flood mask (red) used to delineate the thinned areas of the membrane.

insight into the complex dynamics that underlie the peptide–lipid interactions. By direct inspection of AFM images, we found that the peptides were able to exchange reversibly between the spatially diffuse membrane-thinned state and the highly localized pore state. For example, in Figure 6A,B, the white arrow points to a section of the membrane where the topography changed from a thinned state (panel A) to a pore state (panel B). This change was registered by the membrane going from a shallow depth reading to a deeper depth reading (indicated by the change in color). The circles in Figure 6A–D highlight a region of the bilayer surface that shows that this process is reversible. The circled feature changes its topography from a pore state (panels A and B) to a thinned state (panel C) and then back to a pore state (D). To evaluate this behavior more quantitatively, line scans (Figure 6A′–D′, image panel A corresponds to line scan A′, etc.) show how the feature's depth changes as a function of time. The elapsed time between trace and retrace in the AFM raster scan (red and black in Figure 6A′–D′) was ≤200 ms. We note that the circled feature in Figure 6C,C′ is labeled thin for two reasons: (i) its depth falls within one standard deviation of the membrane thinned peak, and (ii) topographically, it is not highly localized. More generally, this feature could represent a transitional state between the pore state and the thinned state of the membrane.

The time resolution of our AFM (one complete image every 180 s) sets an upper limit to the time scale of the observed topographic state changes. Analysis of 50 individual transitions similar to that circled in Figure 6 revealed that topographic transitions were not observed when examining sequential trace and retrace line scans over nominally the same area of the membrane. This is consistent with the data shown (Figure 6A′–D′) and puts an approximate lower limit of 0.2 s on the time scale to transition between the thinned state and the pore state.

CONCLUSIONS

We provide novel characterization of membrane remodeling induced by the synthetically evolved gain of function peptide MelP5. Direct observations of lipid bilayer remodeling show that MelP5 interacts with the membrane and causes one of two general outcomes that are in equilibrium: delocalized membrane thinning or highly localized pores. We measured the thinning of the bilayer to be approximately 3 Å below the upper leaflet of the bilayer, in overall agreement with previous studies of wild-type melittin. When analyzing pores formed by MelP5, the most probable footprint area was found to be 8.2 nm^2, which gives a most probable radius of 1.7 nm. However, the area histogram exhibited a sizable shoulder and stable pores (on the time scale of image acquisition) were observed with much larger footprint areas, out to about 47 nm^2. Additionally, we have shown that the peptides exchanged reversibly between the thinned state and the pore state and have suggested upper and lower bounds on the characteristic time scale of this transition ($0.2 < \tau < 180$ s). At the P:L ratio we utilized (1:1200) pores were always found surrounded by or abutting thinned areas of the membrane. This is consistent with cooperative pore formation where the local concentration

DOI: 10.1021/acs.langmuir.8b00804
Langmuir 2018, 34, 8393–8399

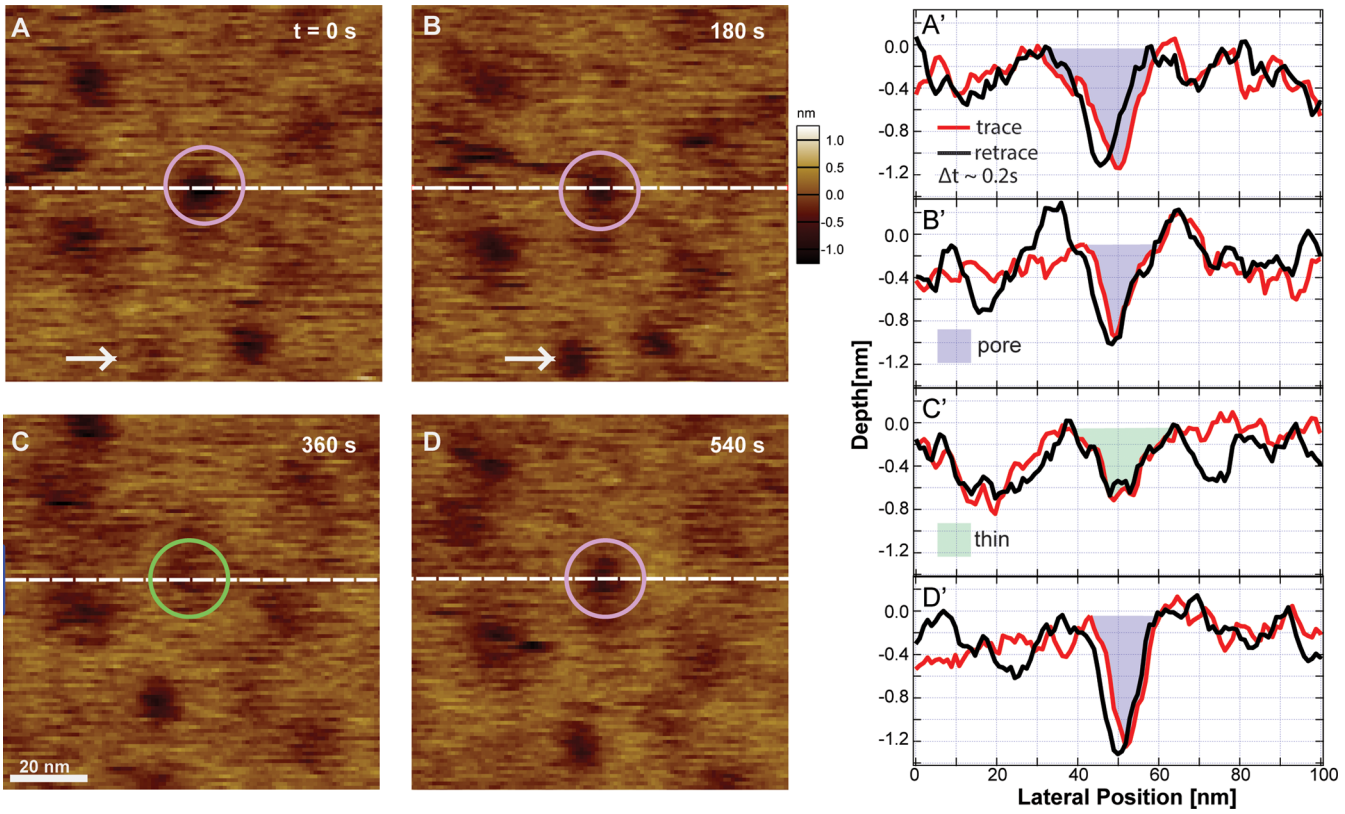

Figure 6. Dynamic transitions of MelP5-induced membrane topography. (A–D) Time lapse images of membrane, arrows and circles highlight interesting features. Line scans from each image (A′–D′, line scan A′ corresponds to image A, etc.) show a detailed view of a transition between a pore state (A, B, D) and a thinned state (C).

of peptides determines the state—inserted or membrane bound—of the peptide.[17] When the local concentration reaches a threshold, a transmembrane pore is created. Under that threshold, the peptides only thin the membrane. In the future it would be interesting to vary the peptide concentration to explore this local thresholding phenomena further. In conclusion, MelP5 has a profound influence on POPC bilayers and AFM imaging provides a direct visualization of the topographic changes imparted by the peptide in a physiologically relevant setting.

MATERIALS AND METHODS

Peptides. MelP5 was synthesized (BioSynthesis Inc.) with a free N-terminus and C-terminal amidation. Identity and purity were verified with HPLC and mass spectrometry. The sequence of MelP5 is GIGAVLKVLATGLPALISWIKAAQQL. Prior to AFM study, the peptide was diluted to a final concentration of 1 μM in imaging buffer: 100 mM NaCl, 50 mM TrisCl at pH 7.4.

Peptide–Lipid Bilayer Preparation. We adopted established methods to form supported lipid bilayers on mica.[29] Briefly, POPC (Avanti Polar Lipids) was suspended in 150 mM NaCl, 40 mM $CaCl_2$, and 20 mM Hepes with a pH of 7.5 at a concentration of 650 μM. Liposomes were prepared by extrusion of POPC through a polycarbonate membrane (approximately 25 times) with a 100 nm pore diameter. POPC liposomes were incubated for 10 min with MelP5 at 25 °C to yield a final peptide concentration of 0.33 μM. The liposomes containing peptides were then deposited onto freshly cleaved mica. Supported bilayers were formed by vesicle fusion (30 min incubation, ~30 °C).[29] Prior to imaging, samples were rinsed (75 μL, four times) with imaging buffer. Unless otherwise specified, experiments were performed at a starting (i.e., prior to rinsing) peptide-to-lipid ratio of 1:1200 and at ~30 °C, significantly above the gel-to-fluid transition temperature of POPC.

AFM Imaging and Analysis. Images were acquired in tapping mode in aqueous buffer solution using a commercial apparatus (Asylum Research, Cypher). Care was taken to control the magnitude of the tip sample force to ≤100 pN (estimated by comparing the free amplitude to the set point amplitude). As is typical, images were flattened (second order) to minimize background. When histograms were compiled, the data were offset so as to align the population having the greatest height (which we assumed to be the unaltered upper surface of the lipid bilayer) to zero. Individual pores were selected using custom software (Igor Pro 7, WaveMetrics), which gave details on the depth and footprint area of each pore.[27] Histograms were fit with multiple Gaussians (MagicPlot), with x_0 defined as the center of the peak.

ASSOCIATED CONTENT

Supporting Information

The Supporting Information is available free of charge on the ACS Publications website at DOI: 10.1021/acs.langmuir.8b00804.

Figures S1–S5 (PDF)

AUTHOR INFORMATION

Corresponding Author

*E-mail: kinggm@missouri.edu (G.M.K.).

ORCID

Gavin M. King: 0000-0002-5811-7012

Present Address

§Department of Applied Physics, Stanford University, Stanford.

Notes

The authors declare no competing financial interest.

DOI: 10.1021/acs.langmuir.8b00804
Langmuir 2018, 34, 8393–8399

■ ACKNOWLEDGMENTS

The authors are grateful to William C. Wimley and Kalina Hristova for stimulating discussions. Additionally, we thank all members of the G. M. King and L. L. Randall research groups at University of Missouri. This work was supported by the National Science Foundation (Award #: 1709792) and the MU Research Board.

■ REFERENCES

(1) Gilbert, R. J. C.; Bayley, H.; Anderluh, G. Membrane pores: from structure and assembly, to medicine and technology. *Philos. Trans. R. Soc., B* **2017**, *372*, 20160208.
(2) Brogden, K. A. Antimicrobial peptides: pore formers or metabolic inhibitors in bacteria? *Nat. Rev. Microbiol.* **2005**, *3*, 238−250.
(3) Soman, N. R.; et al. Molecularly targeted nanocarriers deliver the cytolytic peptide melittin specifically to tumor cells in mice, reducing tumor growth. *J. Clin. Invest.* **2009**, *119*, 2830−2842.
(4) Salomone, F.; et al. A novel chimeric cell-penetrating peptide with membrane-disruptive properties for efficient endosomal escape. *J. Controlled Release* **2012**, *163*, 293−303.
(5) Rausch, J. M.; Marks, J. R.; Rathinakumar, R.; Wimley, W. C. Beta-sheet pore-forming peptides selected from a rational combinatorial library: mechanism of pore formation in lipid vesicles and activity in biological membranes. *Biochemistry* **2007**, *46*, 12124−12139.
(6) Krauson, A. J.; et al. Conformational Fine-Tuning of Pore-Forming Peptide Potency and Selectivity. *J. Am. Chem. Soc.* **2015**, *137*, 16144−16152.
(7) Matin, T. R.; et al. Single-Molecule Peptide-Lipid Affinity Assay Reveals Interplay between Solution Structure and Partitioning. *Langmuir* **2017**, *33*, 4057−4065.
(8) Li, Y.; et al. Single-molecule visualization of dynamic transitions of pore-forming peptides among multiple transmembrane positions. *Nat. Commun.* **2016**, *7*, 12906.
(9) Chen, F.-Y.; Lee, M.-T.; Huang, H. W. Evidence for Membrane Thinning Effect as the Mechanism for Peptide-Induced Pore Formation. *Biophys. J.* **2003**, *84*, 3751−3758.
(10) Hanke, W.; et al. Melittin and a chemically modified trichotoxin form alamethicin-type multi-state pores. *Biochim. Biophys. Acta, Biomembr.* **1983**, *727*, 108−114.
(11) Wiedman, G.; Herman, K.; Searson, P.; Wimley, W. C.; Hristova, K. The electrical response of bilayers to the bee venom toxin melittin: evidence for transient bilayer permeabilization. *Biochim. Biophys. Acta, Biomembr.* **2013**, *1828*, 1357−1364.
(12) Fennouri, A.; Mayer, S. F.; Schroeder, T. B. H.; Mayer, M. Single channel planar lipid bilayer recordings of the melittin variant MelP5. *Biochim. Biophys. Acta, Biomembr.* **2017**, *1859*, 2051−2057.
(13) Yang, Z.; Choi, H.; Weisshaar, J. C. Melittin-Induced Permeabilization, Re-sealing, and Re-permeabilization of E. coli Membranes. *Biophys. J.* **2018**, *114*, 368−379.
(14) Hristova, K.; Dempsey, C. E.; White, S. H. Structure, location, and lipid perturbations of melittin at the membrane interface. *Biophys. J.* **2001**, *80*, 801−811.
(15) van den Bogaart, G.; Guzman, J. V.; Mika, J. T.; Poolman, B. On the mechanism of pore formation by melittin. *J. Biol. Chem.* **2008**, *283*, 33854−33857.
(16) Bechinger, B. The structure, dynamics and orientation of antimicrobial peptides in membranes by multidimensional solid-state NMR spectroscopy. *Biochim. Biophys. Acta, Biomembr.* **1999**, *1462*, 157−183.
(17) Huang, H. W. Molecular mechanism of antimicrobial peptides: the origin of cooperativity. *Biochim. Biophys. Acta, Biomembr.* **2006**, *1758*, 1292−1302.
(18) Wiedman, G.; et al. Highly Efficient Macromolecule-Sized Poration of Lipid Bilayers by a Synthetically Evolved Peptide. *J. Am. Chem. Soc.* **2014**, *136*, 4724−4731.
(19) Woo, S. Y.; Lee, H. Aggregation and insertion of melittin and its analogue MelP5 into lipid bilayers at different concentrations: effects on pore size, bilayer thickness and dynamics. *Phys. Chem. Chem. Phys.* **2017**, *19*, 7195−7203.
(20) Muller, D. J.; Dufrene, Y. F. Atomic force microscopy: a nanoscopic window on the cell surface. *Trends Cell Biol.* **2011**, *21*, 461−469.
(21) Sanganna Gari, R. R.; Frey, N. C.; Mao, C.; Randall, L. L.; King, G. M. Dynamic structure of the translocon SecYEG in membrane: direct single molecule observations. *J. Biol. Chem.* **2013**, *288*, 16848−16854.
(22) Pan, J.; Khadka, N. K. Kinetic Defects Induced by Melittin in Model Lipid Membranes: A Solution Atomic Force Microscopy Study. *J. Phys. Chem. B* **2016**, *120*, 4625−4634.
(23) Cremer, P. S.; Boxer, S. G. Formation and spreading of lipid bilayers on planar glass supports. *J. Phys. Chem. B* **1999**, *103*, 2554−2559.
(24) Chada, N.; et al. Glass is a Viable Substrate for Precision Force Microscopy of Membrane Proteins. *Sci. Rep.* **2015**, *5*, 12550.
(25) van Meer, G.; Voelker, D. R.; Feigenson, G. W. Membrane lipids: where they are and how they behave. *Nat. Rev. Mol. Cell Biol.* **2008**, *9*, 112−124.
(26) Luckey, M. *Membrane Structural Biology*, 2nd ed.; Cambridge University Press: 2014.
(27) Marsh, B. P.; Chada, N.; Sanganna Gari, R. R.; Sigdel, K. P.; King, G. M. The Hessian Blob Algorithm: Precise Particle Detection in Atomic Force Microscopy Imagery. *Sci. Rep.* **2018**, *8*, 978.
(28) King, G. M.; Golovchenko, J. A. Probing nanotube-nanopore interactions. *Phys. Rev. Lett.* **2005**, *95*, 216103.
(29) Mingeot-Leclercq, M. P.; Deleu, M.; Brasseur, R.; Dufrene, Y. F. Atomic force microscopy of supported lipid bilayers. *Nat. Protoc.* **2008**, *3*, 1654−1659.

DOI: 10.1021/acs.langmuir.8b00804
Langmuir 2018, 34, 8393−8399